Applied Mechanics and Materials Vol. 9 (2008) pp. 1-17
online at http://www.scientific.net

Online available since 2007/10/25

Chaotic Zones in Triple Pendulum Dynamics Observed Experimentally and Numerically

Jan Awrejcewicz[a], Grzegorz Kudra[b] and Grzegorz Wasilewski[c]

Department of Automatic and Biomechanics, Technical University of Lodz, Stefanowskiego 1/15, 90-924 Lodz, Poland

[a]awrejcew@p.lodz.pl, [b]grekudra@p.lodz.pl, [c]gwasilew@p.lodz.pl

Keywords: Triple pendulum, experiment, mathematical modeling, parameter estimation, chaotic dynamics

Abstract. The experimental rig of the triple physical pendulum with the first body periodically forced is built. A mathematical model of the real pendulum is created. Friction in joints is modeled as a composition of dry friction and damping. The parameters of the model are estimated matching the output signals from model and experiment. For the minimum searching of the matching function the simplex method is used. Very good agreement between model and real system is obtained. Few chaotic zones are detected numerically and confirmed experimentally.

Introduction

In February, 2005, in the Department of Automatics and Biomechanics, the experimental rig of triple physical pendulum was finished and activated. This stand have been constructed and built in order to investigate experimentally various phenomena of nonlinear dynamics, including regular and chaotic motions, bifurcations, coexisting attractors, etc.

This work is a continuation of earlier studies of authors [1, 2] on a triple physical pendulum. In those studies a numerical model of triple physical pendulum with rigid limiters of motion was formulated. Such a system can exhibit impacts as well as a sliding solutions, with permanent contact with the obstacle on some time intervals. Special numerical tools for non-linear dynamics analysis of that system exhibiting discontinuities was developed and tested. Also the possible application of the numerical model was presented: the piston – connecting rod – crank-shaft system of a combustion engine [1]. On the present stage of investigations the experimental rig of triple pendulum without obstacles is built. The mathematical model presented here is a special case of the models from being studied by us earlier [1, 2].

A pendulum as a simple nonlinear systems is still a subject of interest of scientists from all the world. It is caused by simplicity of that system on the one hand, and due to many fundamental and spectacular phenomena exhibited by a single pendulum on the other hand. In mechanics and physics investigations of single and coupled pendulums are widely applied [3, 4]. Lately, even the monograph on the pendulum have been published [5]. This is a large study on this simple system also from the historical point of view.

The subject of a study can be either a mathematical model or a real physical system. Usually these two objects are investigated simultaneously, and a problem of mathematical model and experimental rig matching arises.

Although a single or a double pendulum (in their different forms) are quite often studied experimentally [6-8], a triple physical pendulum is rather rarely presented in literature from a point of view of real experimental object. For example, in the work [9] the triple pendulum excited by horizontal harmonic motion of the pendulum frame is presented and a few examples of chaotic attractors are reported.

There are two aspects of the interest in the pendulum dynamics. The first one is that the single and coupled pendulums are the very rich sources of many fundamental phenomena of non-linear

dynamics. The second one is the possibility of modeling of many natural and technical objects by the use of system of pendulums. The example is the piston - connecting rod - crankshaft system modeled as a triple physical pendulum with rigid limiters of motion [1].

Experimental Rig

The experimental rig (see Fig. 1) of the triple physical pendulum consists of the following subsystems: pendulum, driving subsystem and the measurement subsystem. It is assumed that the pendulum is moving in a plane.

The links (1, 2, 3) with adjustable lengths and masses are suspended on the frame (4) and joined by the use of radial and axial needle bearings. The first link is forced by a special direct-current motor of our own construction with optical commutation consisting of two stators (6', 6") and two rotors (5', 5"). Both two parts of the motor are structurally symmetrical and electrically coupled. The optical commutator is located on the stator disk (6'). Such a symmetrical drive ensures avoiding the skewing of the structure and forming the forces and moments in planes different that the plane of the assumed pendulum motion. One the other hand such a construction allows the full rotations of the second and the third link of the pendulum.

The voltage conveyed to the engine inductors is controlled by the use of special digital system of our own construction together with precise signal generator HAMEG. As a result the square-shape in time forcing with adjustable frequency and desired amplitude is obtained.

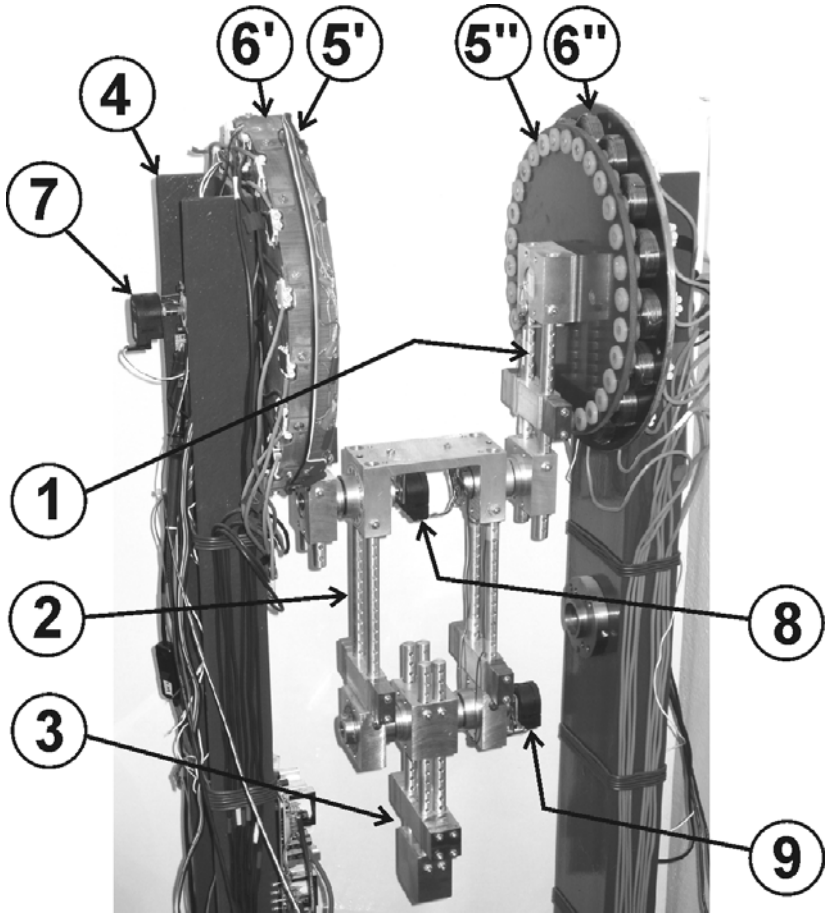

Figure 1. Experimental triple pendulum. 1, 2, 3 – links; 4 – stand; 5',5" – rotors (disk 5' is invisible); 6',6" – stators (disk 6' with optical commutator); 7, 8, 9 – rotational potentiometers.

The measurement of the angular position of the three links is realized by the use of the precise rotational potentiometers (7, 8, 9). Then the LabView measure-programming system is used for experimental data acquisition and presentation on a computer. Detailed description of the triple pendulum construction can be found in the works [10, 11].

Mathematical Modeling

Figure 2 presents an idealized physical concept of the real pendulum presented in Fig. 1. The system is idealized since it is an ideally plane system of coupled rigid links moving in the vacuum. The position of the system is determined by three angles: ψ_1, ψ_2 and ψ_3. The moments of resistance in joints (O_1, O_2 ,O_3) are assumed to be a composition of viscous damping and dry friction with the Stribeck's characteristic. It is assumed to be the same parameters of rotation resistance in each the joint. Each of the pendulums with mass m_i (i =1,2,3) has a mass center lying in the line including the corresponding joints and one of the principal central inertia axes (z_{ci}) of each link is perpendicular to the movement plane x-y. The inertia moment of the i-th link with respect to the axis z_{ci} is I_i (i =1,2,3). The first link is externally forced by the moment $M_e(t)$.

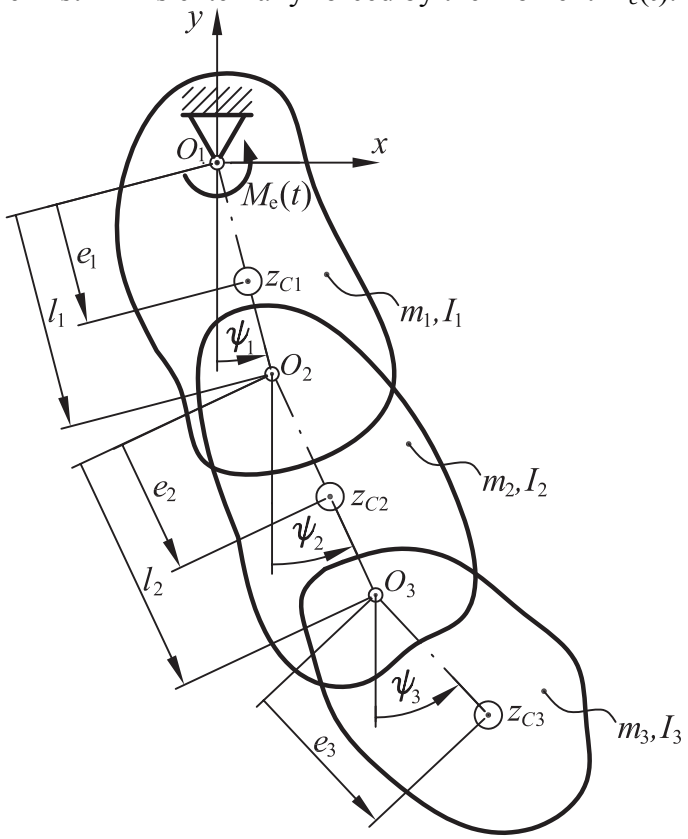

Figure 2. Model of the triple pendulum.

Mathematical description of the above concept of the pendulum follows our earlier works [1-2] where the governing equations of the triple physical pendulum in non-dimensional form have been reported and where only the linear damping in joints have been assumed. The Lagrangian formulation have been used for the derivation of governing equations.

The system is governed by the following set of differential equations:

$$\mathbf{M}(\boldsymbol{\psi})\ddot{\boldsymbol{\psi}} + \mathbf{N}(\boldsymbol{\psi})\dot{\boldsymbol{\psi}}^2 + \mathbf{r}(\boldsymbol{\psi}, \dot{\boldsymbol{\psi}}, \ddot{\boldsymbol{\psi}}) + \mathbf{p}(\boldsymbol{\psi}) = \mathbf{f}_e(t) \tag{1}$$

where

$$\mathbf{M}(\boldsymbol{\psi})=\begin{bmatrix} B_1 & N_{12}\cos(\psi_1-\psi_2) & N_{13}\cos(\psi_1-\psi_3) \\ N_{12}\cos(\psi_1-\psi_2) & B_2 & N_{23}\cos(\psi_2-\psi_3) \\ N_{13}\cos(\psi_1-\psi_3) & N_{23}\cos(\psi_2-\psi_3) & B_3 \end{bmatrix},$$

$$\mathbf{N}(\boldsymbol{\psi})=\begin{bmatrix} 0 & N_{12}\sin(\psi_1-\psi_2) & N_{13}\sin(\psi_1-\psi_3) \\ -N_{12}\sin(\psi_1-\psi_2) & 0 & N_{23}\sin(\psi_2-\psi_3) \\ -N_{13}\sin(\psi_1-\psi_3) & -N_{23}\sin(\psi_2-\psi_3) & 0 \end{bmatrix}, \tag{2}$$

$$\mathbf{p}(\boldsymbol{\psi})=\begin{Bmatrix} M_1\sin\psi_1 \\ M_2\sin\psi_2 \\ M_3\sin\psi_3 \end{Bmatrix},\quad \mathbf{f}_e(t)=\begin{Bmatrix} M_e(t) \\ 0 \\ 0 \end{Bmatrix},\qquad \boldsymbol{\psi}=\begin{Bmatrix} \psi_1 \\ \psi_2 \\ \psi_3 \end{Bmatrix},\quad \dot{\boldsymbol{\psi}}=\begin{Bmatrix} \dot{\psi}_1 \\ \dot{\psi}_2 \\ \dot{\psi}_3 \end{Bmatrix},\quad \ddot{\boldsymbol{\psi}}=\begin{Bmatrix} \ddot{\psi}_1 \\ \ddot{\psi}_2 \\ \ddot{\psi}_3 \end{Bmatrix},\quad \dot{\boldsymbol{\psi}}^2=\begin{Bmatrix} \dot{\psi}_1^2 \\ \dot{\psi}_2^2 \\ \dot{\psi}_3^2 \end{Bmatrix}.$$

The denotations used above have the following meaning:

$$B_1=I_1+e_1^2m_1+l_1^2(m_2+m_3),\quad B_2=I_2+e_2^2m_2+l_2^2m_3,\quad B_3=I_3+e_3^2m_3,$$

$$N_{12}=m_2e_2l_1+m_3l_1l_2,\quad N_{13}=m_3e_3l_1,\quad N_{23}=m_3e_3l_2, \tag{3}$$

$$M_1=m_1ge_1+(m_2+m_3)gl_1,\quad M_2=m_2ge_2+m_3gl_2,\quad M_3=m_3ge_3,$$

where g=9.81 m/s^2 is the gravitational acceleration.

The vector of generalized forces **r** is a vector of forces appearing in relation to the resistance in joints and has the following form

$$\mathbf{r}(\boldsymbol{\psi},\dot{\boldsymbol{\psi}},\ddot{\boldsymbol{\psi}})=\begin{Bmatrix} M_{R1}-M_{R2} \\ M_{R2}-M_{R3} \\ M_{R3} \end{Bmatrix}, \tag{4}$$

where M_{ri} (i=1, 2, 3) is a resistance moment in i-th joint, composed of two parts:

$$M_{Ri}=M_{Ti}+M_{Di}\qquad (i=1,2,3), \tag{5}$$

In Eq. 5 M_{Di} is a viscous damping moment with common for all joints coefficient c:

$$M_{D1}=c\dot{\psi}_1,\quad M_{D2}=c(\dot{\psi}_2-\dot{\psi}_1),\quad M_{D3}=c(\dot{\psi}_3-\dot{\psi}_2), \tag{6}$$

and M_{Ti} is moment of dry friction modeled in the following way:

$$M_{Ti}=\operatorname{sign}(\omega_{rel(i)})\,\mu_r(\omega_{rel(i)})N_i, \tag{7}$$

where $\omega_{rel(i)}$ is a relative angular velocity in *i*-th joint:

$$\omega_{rel(1)} = \dot{\psi}_1, \quad \omega_{rel(2)} = \dot{\psi}_2 - \dot{\psi}_1, \quad \omega_{rel(3)} = \dot{\psi}_3 - \dot{\psi}_2 . \tag{8}$$

N_i is a reaction force in *i*-th joint, whereas $\mu_r = \mu r$ is a dry friction coefficient μ multiplied by the bearing radius *r* being common for all joints.

The dry friction coefficient μ_r is assumed to be dependent on relative angular velocity according to Stribeck's curve:

$$\mu_r\left(\omega_{rel}\right) = \left(\mu_{r0} - \mu_{rG}\right)\exp\left(\frac{-c_{Str}\left|\omega_{rel}\right|}{\mu_{r0} - \mu_{rG}}\right) + \mu_{rG}, \tag{9}$$

where μ_{r0} is dry friction coefficient for $\omega_{rel} = 0$, μ_{rG} is dry friction coefficient for $\omega_{rel} \to \pm\infty$ and c_{Str} are parameters describing how fast the function $\mu_r(\omega_{rel})$ reaches the μ_{rG} as $|\omega_{rel}|$ increases.

The reaction forces in bearings are

$$N_1 = \sqrt{N_{1n}^2 + N_{1t}^2}, \quad N_2 = \sqrt{N_{2n}^2 + N_{2t}^2}, \quad N_3 = \sqrt{N_{3n}^2 + N_{3t}^2}, \tag{10}$$

where:

$$\begin{aligned}
N_{3n} &= m_3\Big[g\cos\psi_3 + e_3\dot{\psi}_3^2 + l_1\left(\ddot{\psi}_1\sin\left(\psi_1 - \psi_3\right) + \dot{\psi}_1^2\cos\left(\psi_1 - \psi_3\right)\right) + \\
&\quad + l_2\left(\ddot{\psi}_2\sin\left(\psi_2 - \psi_3\right) + \dot{\psi}_2^2\cos\left(\psi_2 - \psi_3\right)\right)\Big], \\
N_{3t} &= m_3\Big[g\sin\psi_3 + e_3\ddot{\psi}_3 + l_1\left(\ddot{\psi}_1\cos\left(\psi_1 - \psi_3\right) - \dot{\psi}_1^2\sin\left(\psi_1 - \psi_3\right)\right) + \\
&\quad + l_2\left(\ddot{\psi}_2\cos\left(\psi_2 - \psi_3\right) - \dot{\psi}_2^2\sin\left(\psi_2 - \psi_3\right)\right)\Big], \\
N_{2n} &= m_2\Big[g\cos\psi_2 + e_2\dot{\psi}_2^2 + l_1\left(\ddot{\psi}_1\sin\left(\psi_1 - \psi_2\right) + \dot{\psi}_1^2\cos\left(\psi_1 - \psi_2\right)\right)\Big] + \\
&\quad + N_{3n}\cos\left(\psi_2 - \psi_3\right) - N_{3t}\sin\left(\psi_2 - \psi_3\right), \\
N_{2t} &= m_2\Big[g\sin\psi_2 + e_2\ddot{\psi}_2 + l_1\left(\ddot{\psi}_1\cos\left(\psi_1 - \psi_2\right) - \dot{\psi}_1^2\sin\left(\psi_1 - \psi_2\right)\right)\Big] + \\
&\quad + N_{3n}\sin\left(\psi_2 - \psi_3\right) + N_{3t}\cos\left(\psi_2 - \psi_3\right), \\
N_{1n} &= m_1\left[g\cos\psi_1 + e_1\dot{\psi}_1^2\right] + N_{2n}\cos\left(\psi_1 - \psi_2\right) - N_{2t}\sin\left(\psi_1 - \psi_2\right), \\
N_{1t} &= m_1\left[g\sin\psi_1 + e_1\ddot{\psi}_1\right] + N_{2n}\sin\left(\psi_1 - \psi_2\right) + N_{2t}\cos\left(\psi_1 - \psi_2\right).
\end{aligned} \tag{11}$$

The external excitation of the pendulum is assumed to be an ideal square shape function of time:

$$M_e\left(t\right) = q\,\mathrm{sign}\left(\sin\left(\omega t + \phi_0\right)\right) \tag{12}$$

with amplitude q, angular velocity ω and with initial phase ϕ_0.

In order to make easier the problem of numerical solving the Eq. 1, the sign function in Eq. 7 is approximated by the use of arctan function and the Eq. 7 takes the form:

$$M_{Ti} = \frac{2}{\pi}\arctan\left(\varepsilon\,\omega_{rel(i)}\right)\mu_r\left(\omega_{rel(i)}\right)N_i\,, \tag{13}$$

where ε is a parameter. The simulations presented in this paper are performed for ε=1000. Thanks to this approximation, there is no need for detection of the points of discontinuity of Eq. 7 during the simulation. Instead of this, the integration method with variable step and with the control of the estimated error is used. The error is estimated by comparison of results obtained by the use of two methods: four-order Runge-Kutta method and five-order Runge-Kutta method. Last method is then applied to solve the differential equations. The discontinuity points in Eq. 12 are detected, because we do not smooth the corresponding function.

Here we address another problem related to numerical solving the governing Eq. 1. When we use numerical methods we need to solve Eq. 1 algebraically with respect to $\ddot{\boldsymbol{\psi}}$. Since the dry friction moments depend on normal reactions in joints (terms in vector **r**), these equations are non-linear and we must use a numerical technique. The Newton method is taken and we need to know Jacobian of the corresponding non-linear function. This implies another problem, regarding of quite complex analytical form of the Jacobian. Observe that there is no need to have this analytical form or even to compute it numerically. We use approximate analytical form of Jacobian, namely $\mathbf{M}(\boldsymbol{\psi})$ according to Eq. 2, which differs not much from full Jacobian, and gives fast convergence of the Newton method. This is a very efficient way to deal with solution to Eq. 1.

Experimental and Numerical Investigations

Mathematical model built so far requires knowledge of the parameter values to perform numerical simulations. Although it is possible to measure and calculate all mass and length parameters of the pendulum, however for some parameters it would be quite work-consuming or not enough accurate. Therefore we measure only two parameters:

$$l_1 = 0.174\ \text{[m]},\ l_2 = 0.225\ \text{[m]} \tag{14}$$

and we assume also g=9.81 m/s^2. The vector of remaining parameters follows

$$\boldsymbol{\mu} = \left[m_1, m_2, m_3, I_1, I_2, I_3, e_1, e_2, e_3, c, \mu_{r0}, \mu_{rG}, c_{Str}\right]. \tag{15}$$

The model parameters are then estimated by the global minimum searching of the criterion-function of the model and real system matching. The matching of model and real system is understood as the matching of the corresponding output signals $\psi_i(t)$ (i=1,2,3) from model integrated numerically and from the real pendulum, assuming the same inputs (external forcing $M_e(t)$) to both model and real system. The sum of squares of deviations between corresponding samples of signals from model and experiment, for few different solutions, serves as a criterion function. Together with the model parameters also initial conditions of the numerical simulation are estimated. A minimum is searched applying the simplex method. In order to avoid the local minima, the simplex method is stopped from time to time and a random searching is then applied. After random searching the simplex method is restarted again.

For the parameters estimation four periodic experimental series are used for different forcing frequencies f = 0.35, 0.6, 0.85 and 1.1 Hz ($f=\omega/(2\pi)$) and for the same forcing amplitude q = 2 Nm. The experimental series are registered during time interval of length equal to 20 s. The numerical

simulation is performed with the forcing exactly the same as excitation applied in real system for each periodic solution saved. Note that the dimension of the problem is now equal to 37 (length of the parameter vector (13) plus number of initial conditions for four solutions (24)).

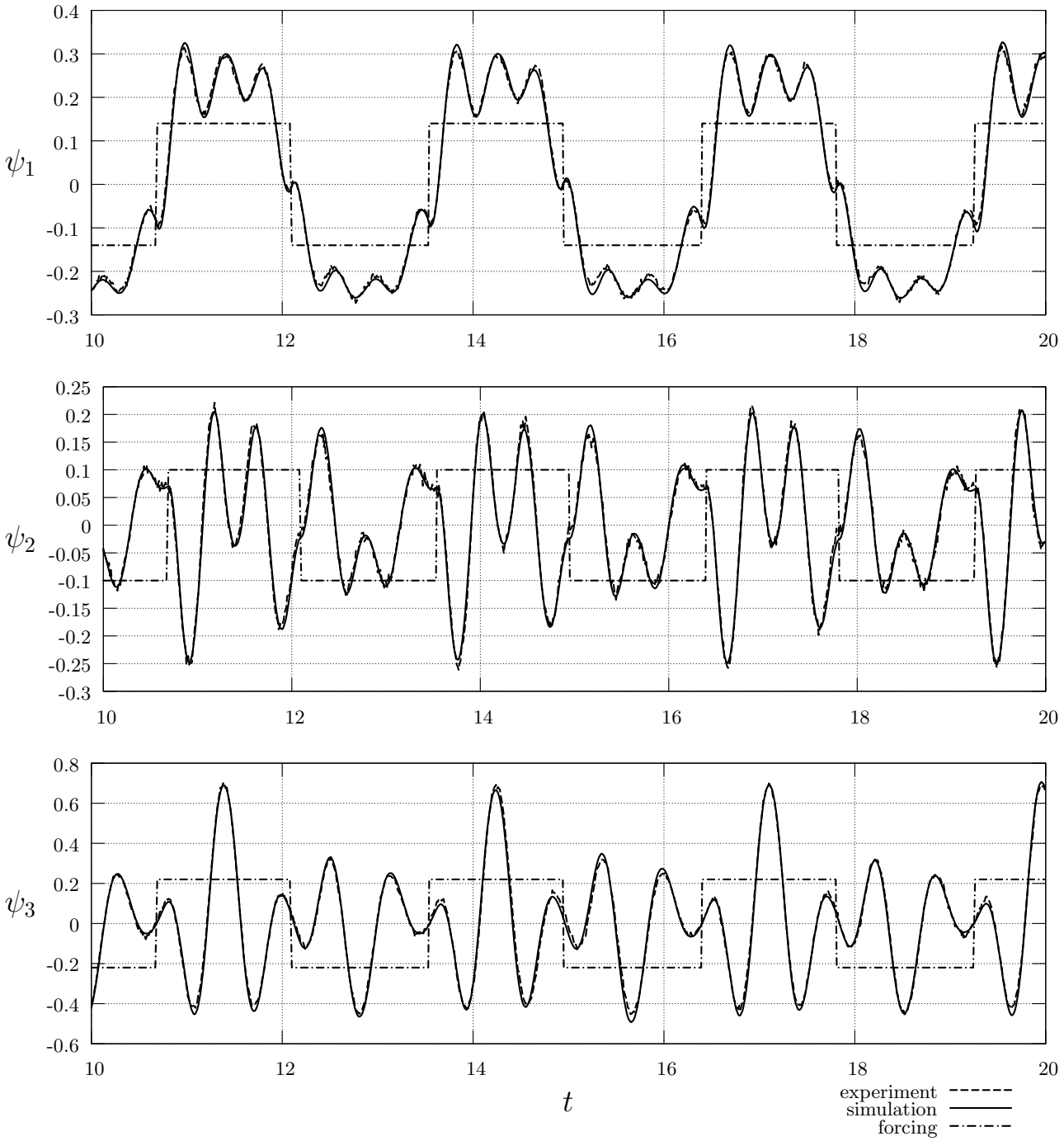

Figure 3. Periodic solution for forcing frequency f = 0.35 Hz observed experimentally and numerically.

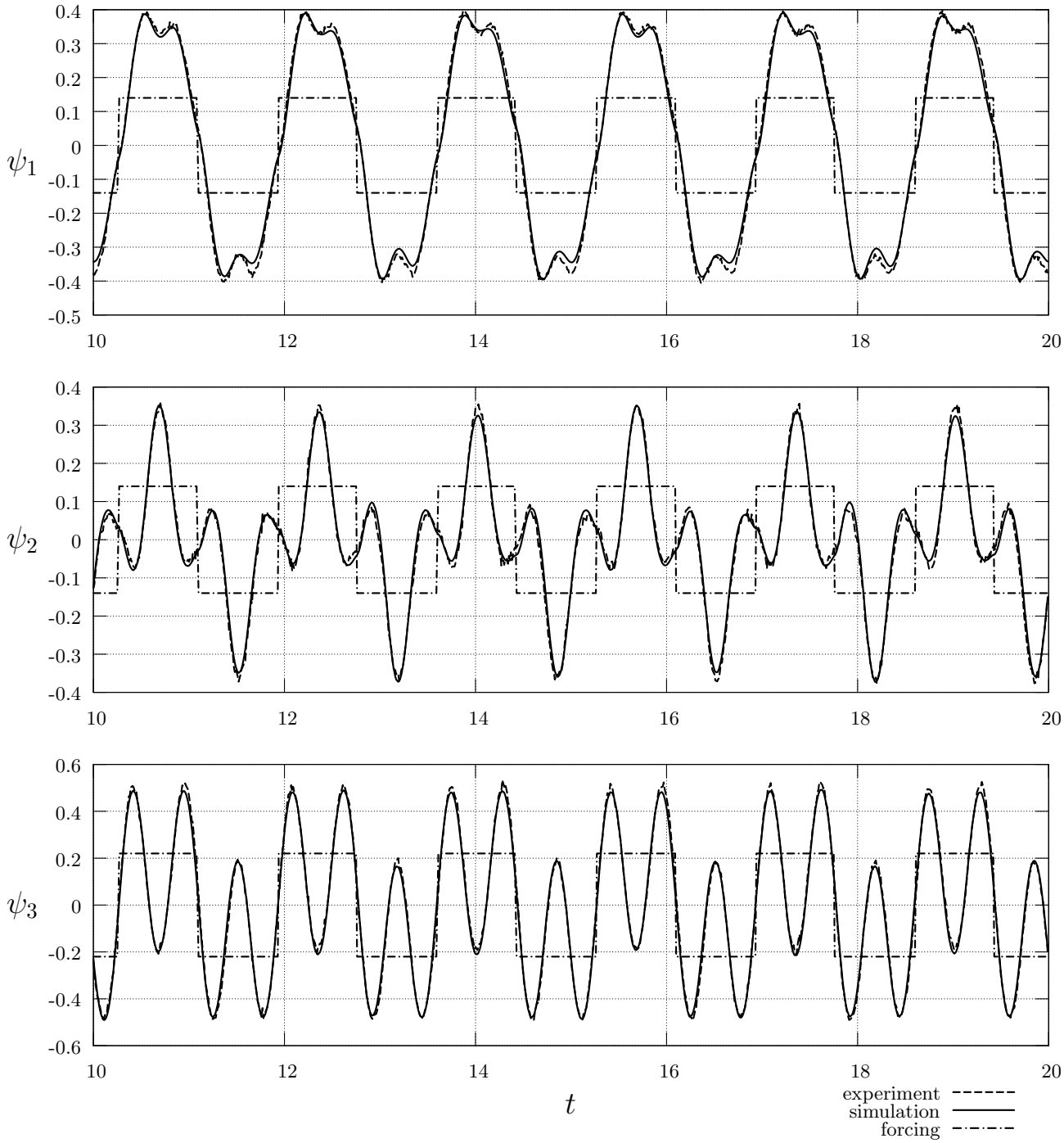

Figure 4. Periodic solution for forcing frequency $f = 0.6$ Hz observed experimentally and numerically.

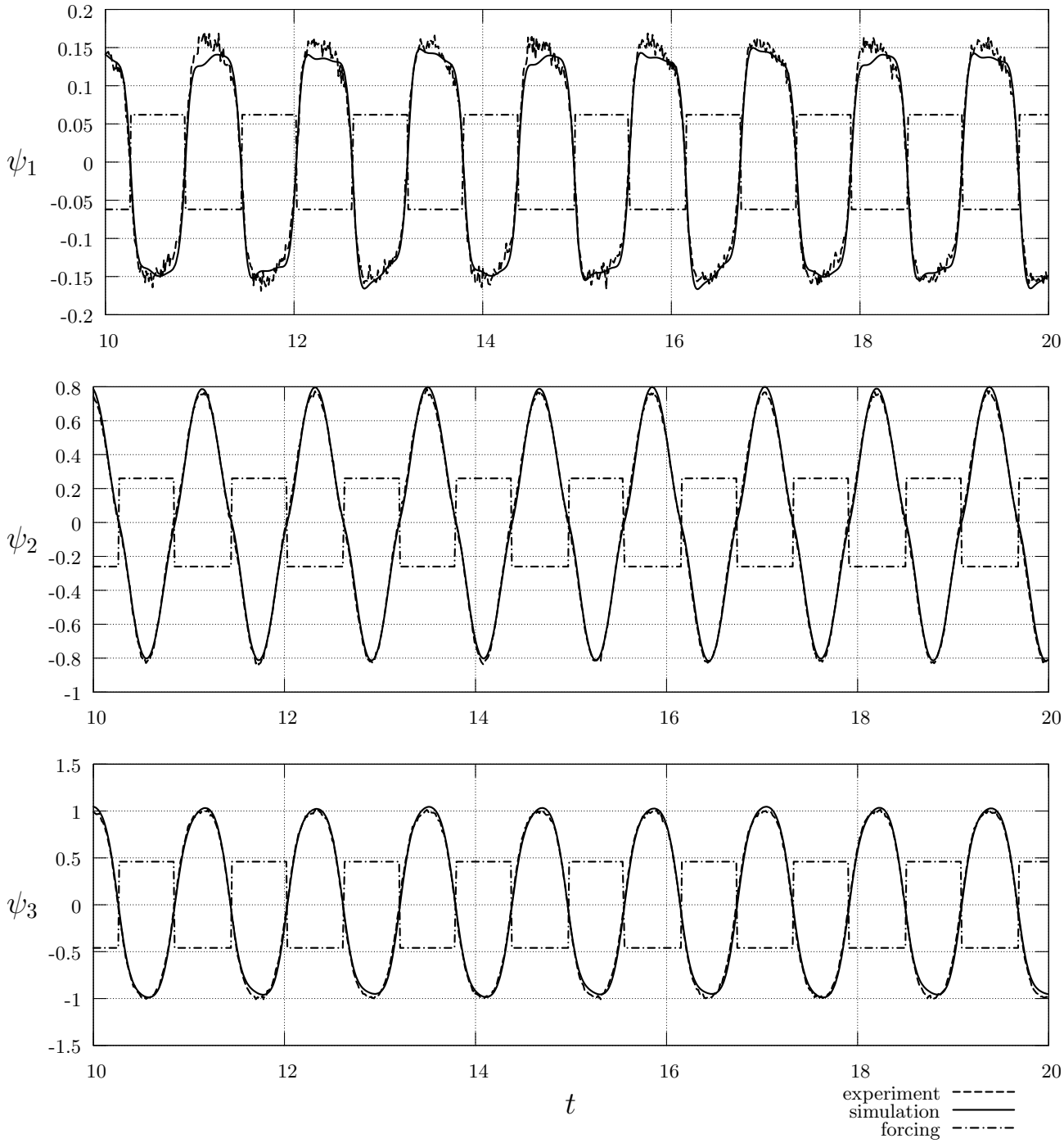

Figure 5. Periodic solution for forcing frequency f = 0.85 Hz observed experimentally and numerically.

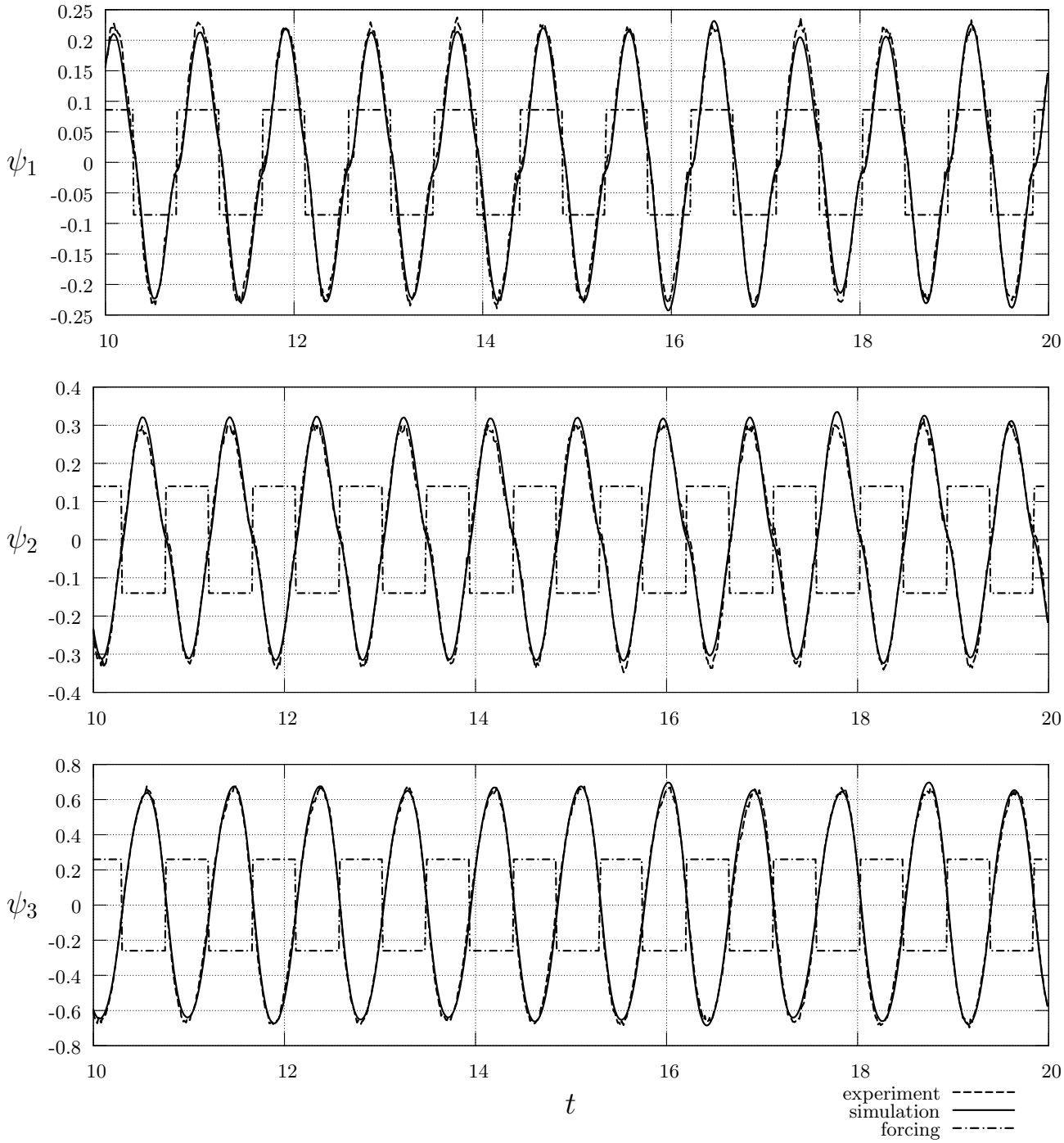

Figure 6. Periodic solution for forcing frequency f = 1.1 Hz observed experimentally and numerically.

The following set of parameters is obtained:

$$m_1 = 2.908\ [\mathrm{kg}],\quad m_2 = 2.266\ [\mathrm{kg}],\quad m_3 = 2.601\ [\mathrm{kg}],$$

$$I_1 = 0.03159\ [\mathrm{kg\,m^2}],\quad I_2 = 0.01847\ [\mathrm{kg\,m^2}],\quad I_3 = 0.01230\ [\mathrm{kg\,m^2}],$$

$$e_1 = 0.06687\ [\mathrm{m}],\quad e_2 = 0.06866\ [\mathrm{m}],\quad e_3 = 0.05138\ [\mathrm{m}], \tag{16}$$

$$c = 3.684\cdot 10^{-4}\ [\mathrm{kg\,m^2 s^{-1}}],$$

$$\mu_{r0} = 6.521\cdot 10^{-4}\ [\mathrm{m}],\quad \mu_{rG} = 6.055\cdot 10^{-4}\ [\mathrm{m}],\quad c_{Str} = 0.9042\ [\text{-}],$$

which corresponds to the model and real system output signals matching presented in Figs 3-6, where solutions are presented only for last 10 s. If we divide final value of criterion-function by the number of samples used in calculation of criterion-function, we obtain average square of deviation between two signals obtained: from the model and the experiment. Let us denote this parameter as ASD (average squared deviation). Now this parameter can be used for comparison of matching of different sets of experimental data and numerical solutions. For solutions presented in Figs 3-6 we have ASD=$0.3805\cdot 10^{-3}$ [rad^2].

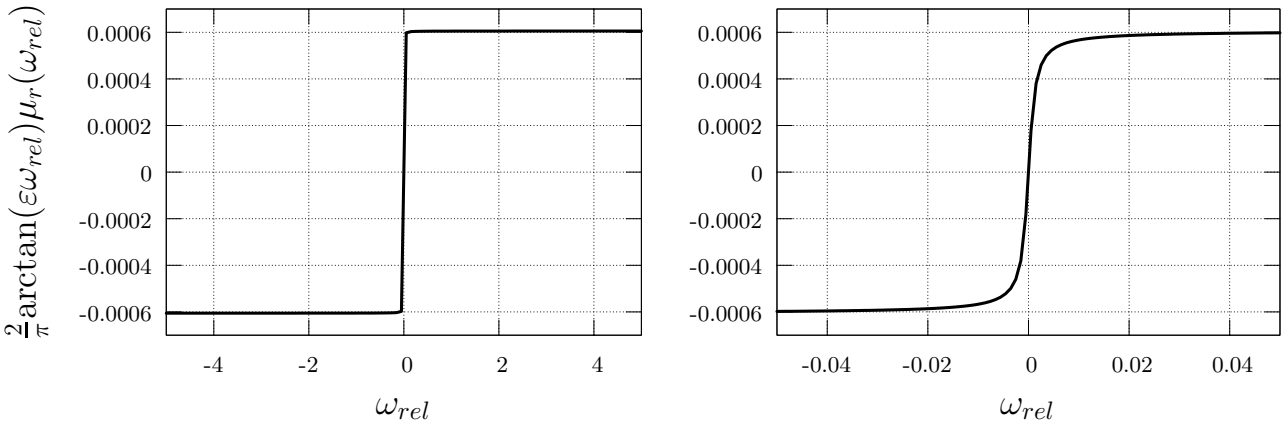

Figure 7. Dry friction characteristics for ε=1000 and other parameters according to Eq. 17.

In Fig. 7 we have presented dry friction characteristic for ε=1000 and other parameters estimated (according to Eq. 17). Observe, that because of approximation, some parts of characteristic are cut of. Namely, we do not observe static friction coefficient (μ_{r0}=$6.521\cdot 10^{-4}$ m) larger than friction coefficient for $\omega_{rel} \to \pm\infty$ (μ_{rG}=$6.055\cdot 10^{-4}$ m). In this situation the value of μ_{r0} coefficient plays no role as well as c_{Str} coefficient has no significance on simulations presented in this paper.

In Figs 8-9 there are presented characteristics of dry friction moments M_{Ti} and damping moments M_{Di} (straight lines) as well as characteristics of reaction force N_i for each the joint (i=1,2,3). We have presented these characteristics for two cases: for periodic solution in Fig. 8 (f = 0.6 Hz) and for chaotic solution in Fig. 9 (f = 0.73 Hz). We can compare moments generated by damping and moments generated by dry friction. Note that damping can be practically neglected for the first joint (point O_1), for the second joint (O_2) the influence of damping is larger and for the third one (O_3) the damping plays significant role. We can also observe the values reaction forces in particular joints for different solutions. Namely, for periodic solution with forcing frequency f = 0.6 Hz these forces

can reach ~83 N, whereas for chaotic one with forcing frequency f = 0.73 Hz these forces can reach even ~1100 N (for the first joint).

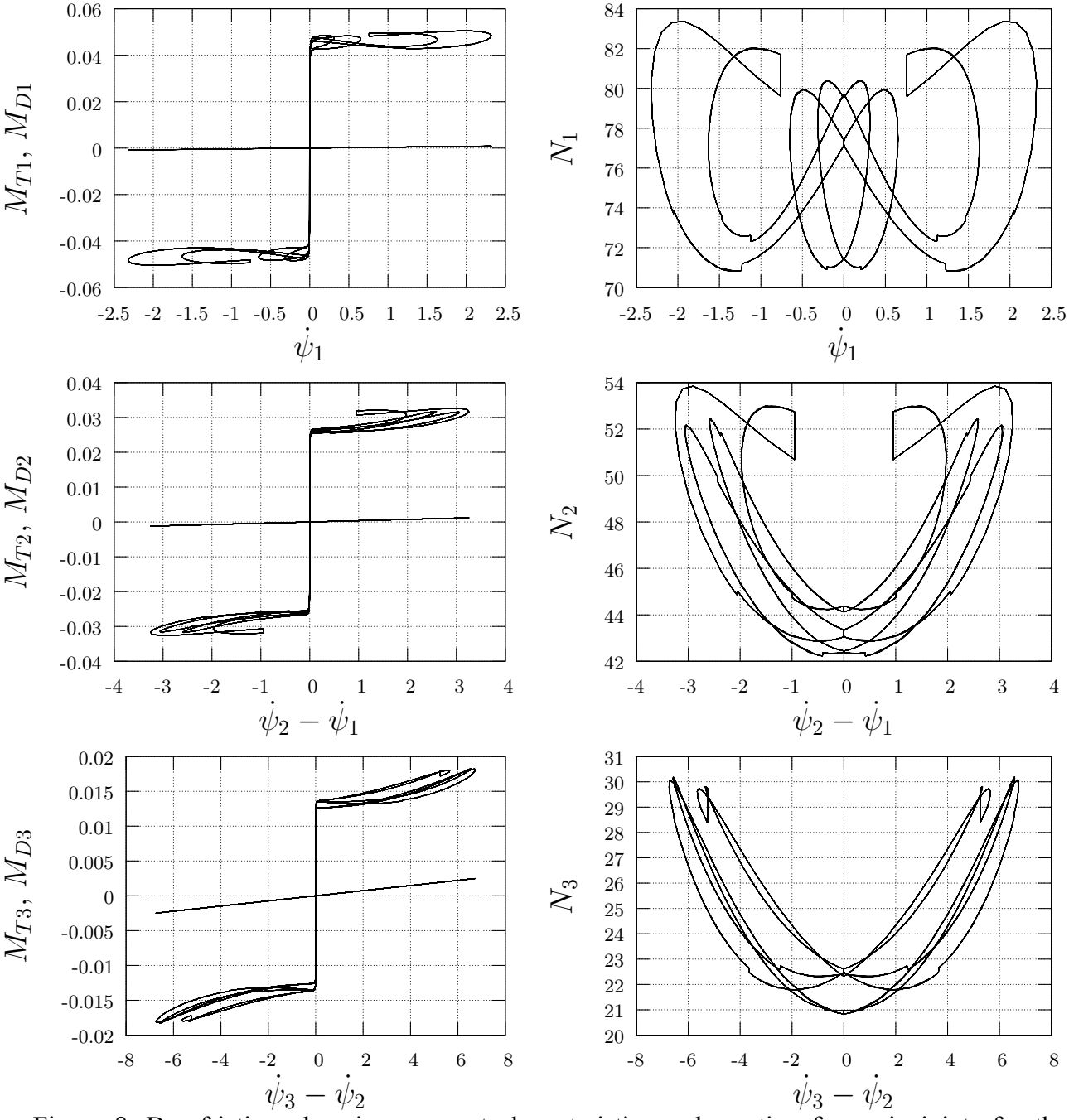

Figure 8. Dry friction, damping moment characteristics and reaction forces in joints for the periodic model response (f = 0.6 Hz).

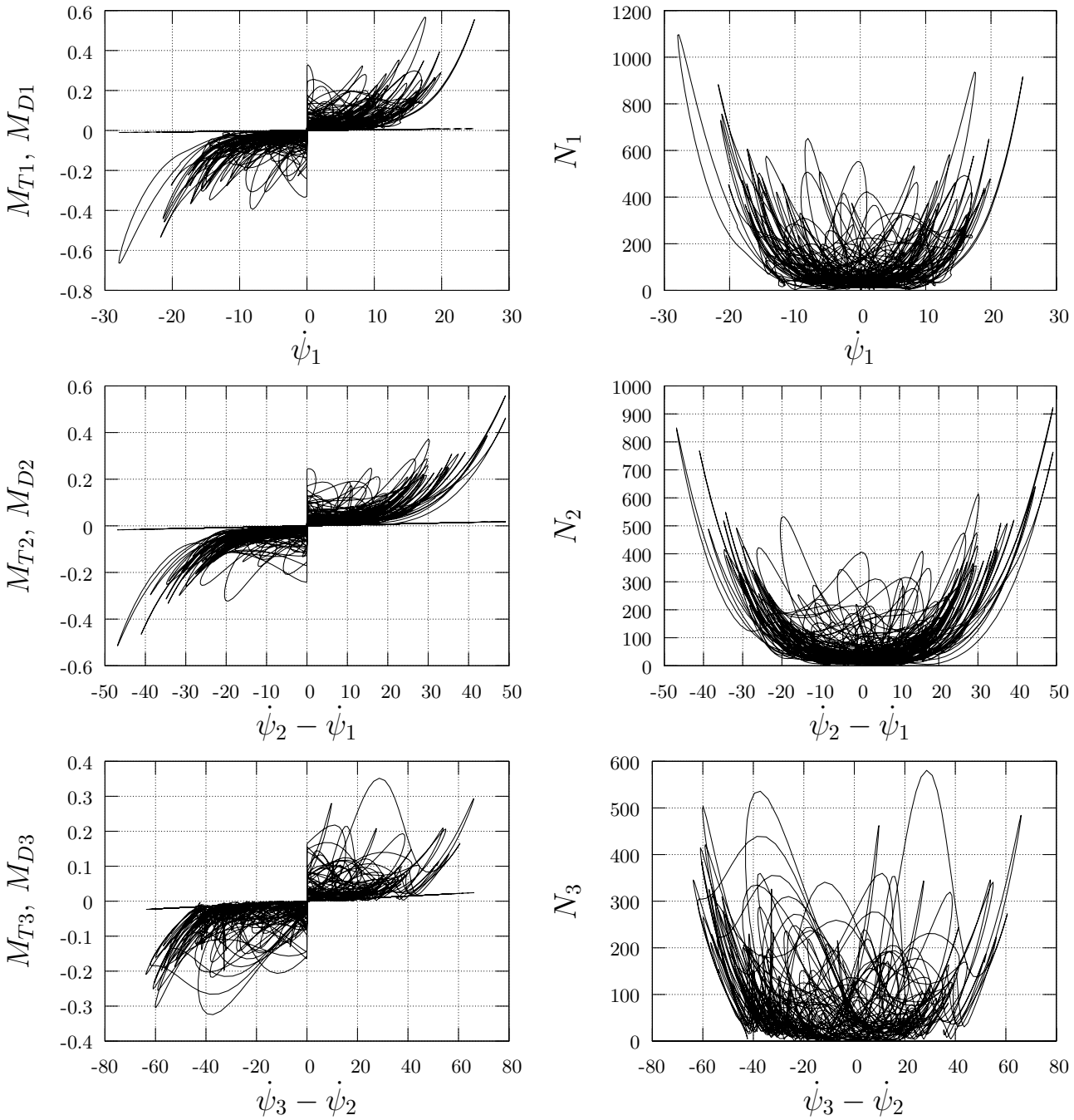

Figure 9. Dry friction, damping moment characteristics and reaction forces in joints for the chaotic model response (f = 0.73 Hz).

Figure 10 contains a bifurcation diagram for the mathematical model with the forcing frequency f as a bifurcation parameter. The diagram was performed for the frequency growing from 0.35 Hz to 1.1 Hz. Chaotic windows are observed numerically for $f\in(0.395,0.400)$ (zone I), for $f\in(0.631,0.645)$ (zone II) and $f\in(0.695,0.779)$ (zone III). However, this bifurcation diagram is only for growing parameter and these chaotic zones may be larger (in some regions a few solutions can coexist, for example both chaotic and periodic ones). These three zones are also observed experimentally in regions approximately the same as shown in Fig. 10. In addition, full rotations performed by individual links observed in particular zones of numerical bifurcation diagram are experimentally confirmed. Note that in zones I and II only the third link performs full rotations, whereas in zone III all links perform full rotations.

Figure 11 presents comparison of chaotic solutions for forcing frequency f = 0.73 Hz obtained experimentally and numerically. Both solutions start from the same initial conditions and their

divergence can be observed. Figure 12 contains projections of the Poincaré section of the attractor of the mathematical model for f = 0.73 Hz.

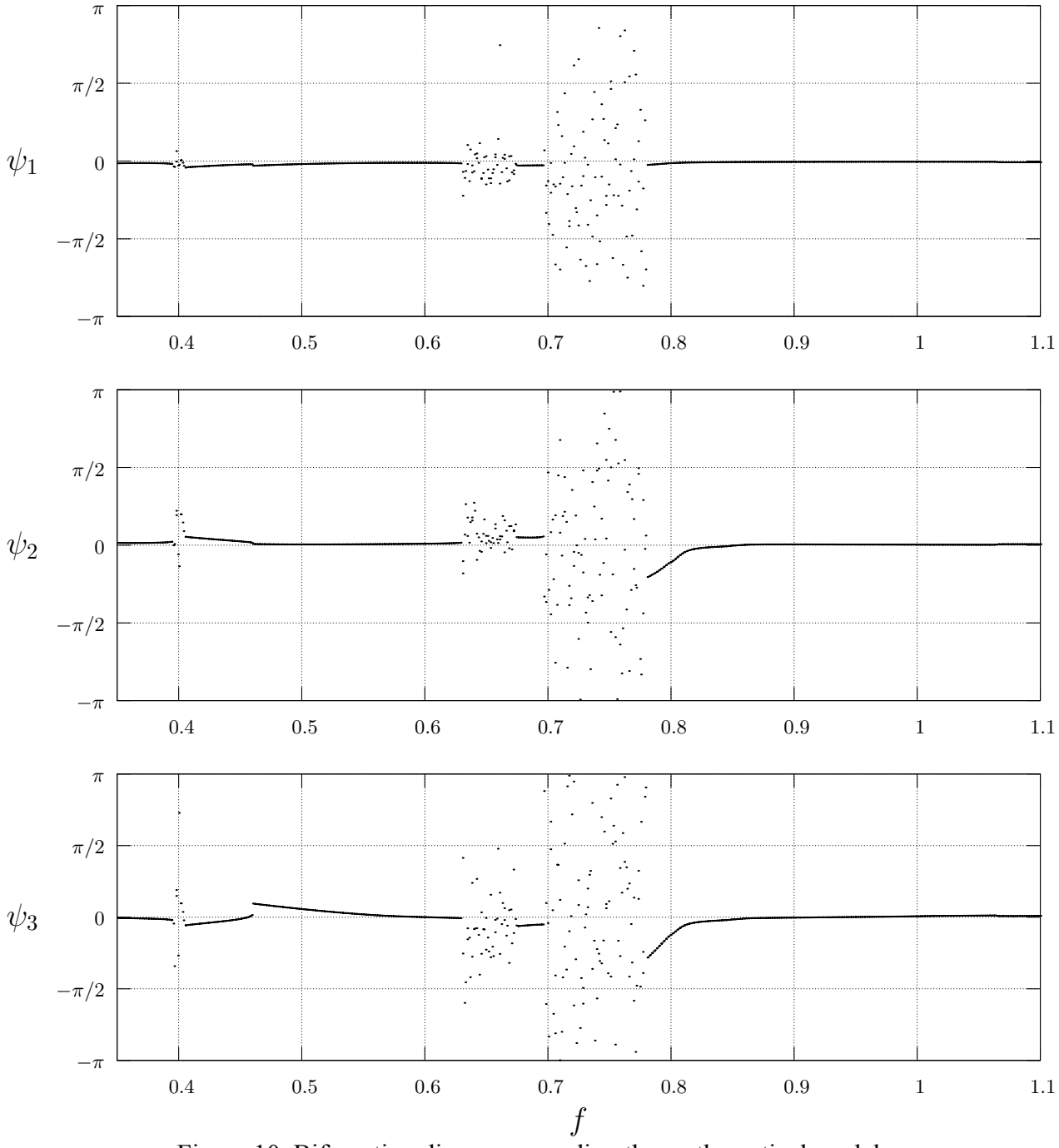

Figure 10. Bifurcation diagram regarding the mathematical model.

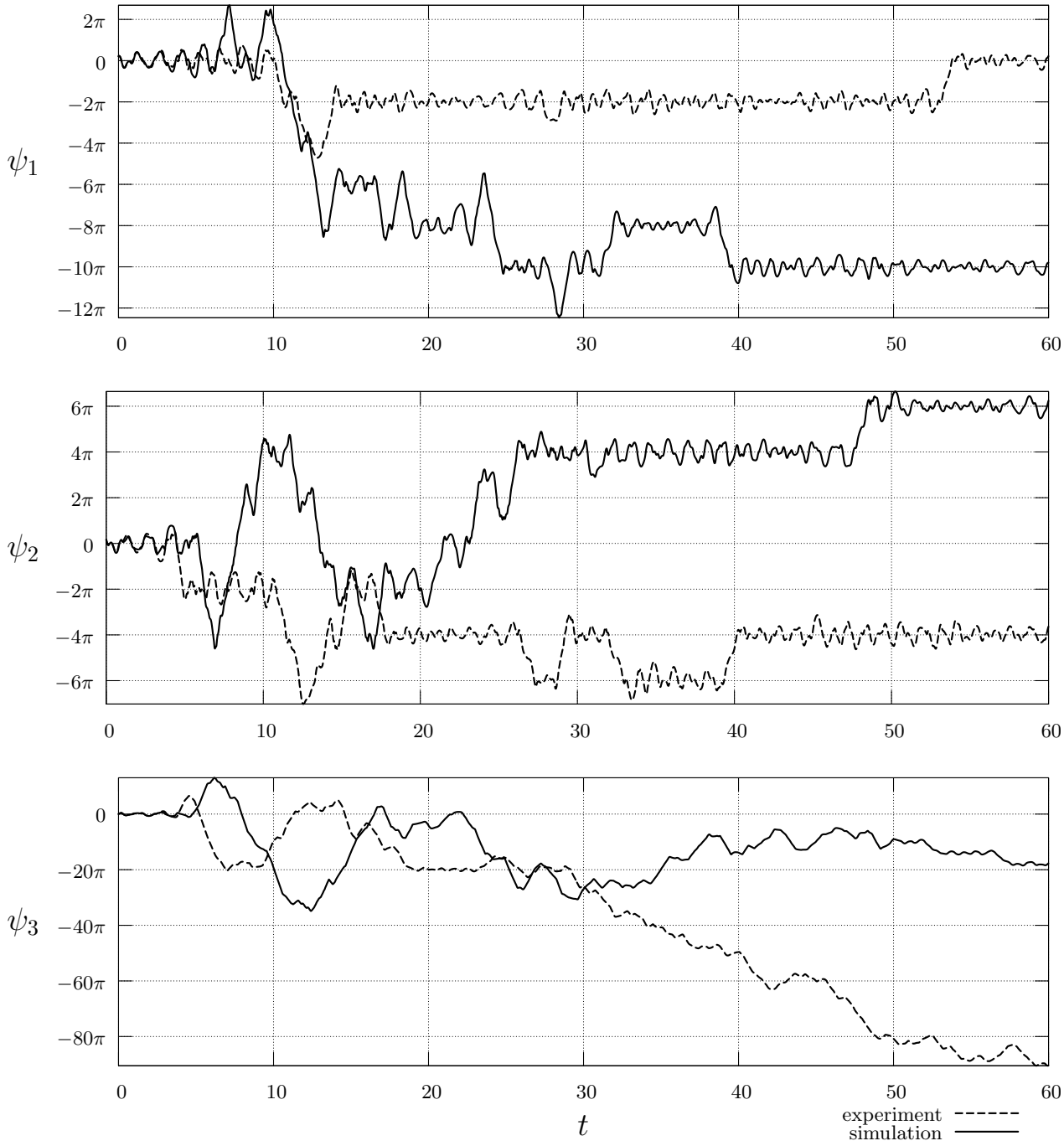

Figure 11. Chaotic solution for forcing frequency f = 0.73 Hz observed experimentally and numerically.

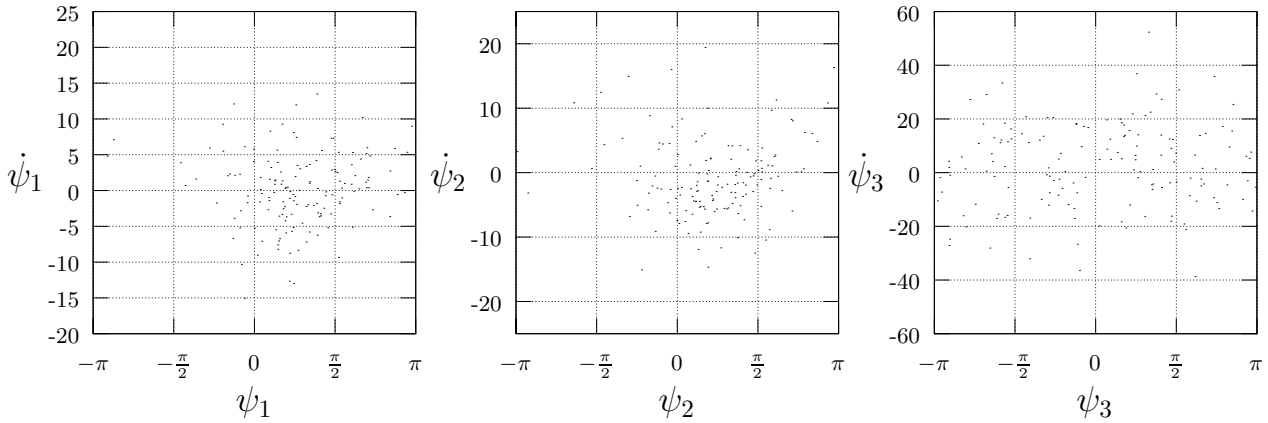

Figure 12. Projections of the Poincaré section of the chaotic solution exhibited by the mathematical model for forcing frequency f = 0.73 Hz.

Concluding Remarks

Good agreement between both numerical simulation results and experimental measurements have been obtained and presented. A few chaotic zones have been detected and confirmed well by the experiment. Experiment verifies positively the boundaries of the particular chaotic windows as well as some qualitative features of chaotic solutions like performing (or not) the full rotations by individual links. It leads to conclusion that the used mathematical model of triple pendulum with its parameters estimated can be applied as a tool for quick searching for various phenomena of nonlinear dynamics exhibited by a real pendulum as well as for explanation of its rich dynamics.

It should be noted that because of the method of parameter estimation used, the model parameter values are not optimal in the sense of the best real physical values approximation, but rather in the sense of the best matching of output signals from the model and the real pendulum.

There may be two sources of differences between results of numerical simulation and experimental observations. Firstly, the mathematical model may be not sufficiently complex for describing some real physical phenomena in the triple pendulum. Secondly, the method of global minimum finding, for the criterion-function, in the case of multi-dimensional problem (the simplex method) does not belong to perfect ones. In other words sometimes it is not clear, that we have found a global minimum and not just a local one.

The first reason of differences between model and reality in our case, however, seems to be more important. Especially the friction model may be developed in order to obtain better results. For example, one idea is to make assumption, that the friction and damping in the first joint have their own parameters independent from the parameters of motion resistances in other joints. It can be justified by a special work conditions of the first joint bearings, because of nearness of the motor producing some quantities of heat. The second idea is to develop the friction model itself. It may happen that the used Stribeck's characteristic is not sufficient for describing friction phenomena proceeding in bearings for full range of relative angular velocities.

Acknowledgments

This work has been supported by the Ministry of Science and Information (grant No 4 T07A 031 28).

References

[1] J. Awrejcewicz and G. Kudra: Int. J. Bifurcation and Chaos Vol. **15**(7) (2005), p. 2207.

[2] J. Awrejcewicz, G. Kudra and C.-H. Lamarque: Int. J. Bifurcation and Chaos Vol. **14**(2) (2004), p. 4191.

[3] A. C. Skeledon and T. Mulline: Phys. Lett. Vol. **A166** (1992), p. 224.

[4] A. C. Skeledon: Physica Vol. **D75** (1994), p. 541.

[5] G. L. Baker and J. A. Blackburn: *The Pendulum. A Case Study in Physics* (Oxford University Press, 2005).

[6] J. A. Blackburn, Y. Zhou-Jing, H. J. Smith and M. A. H. Nerenberg: Physica Vol. **D26** (1987), p. 385.

[7] H. Heng, R. Doerner, B. Hubinger and W. Martienssen: Int. J. Bifurcation and Chaos Vol. **4**(4) (1994), p. 751.

[8] S. R. Bishop and M. J. Clifford: J. Sound and Vib. Vol. **189**(1) (1996), p. 142.

[9] Q. Zhu and M. Ishitobi: J. Sound and Vib. Vol. **227**(1) (1999), p. 230.

[10] B. Supeł: *Experimental Investigations and Numerical Analysis of Simple Chaotic Mechanical Models* (Ph.D. Thesis, Technical University of Lodz, Poland 2005, in Polish).

[11] J. Awrejcewicz, B. Supeł, G. Kudra, G. Wasilewski and P. Olejnik, in: Proceedings of Fifth EUROMECH Nonlinear Dynamics Conference, p. 1817, The Netherlands (2005).